Earth and Planetary Science Letters 429 (2015) 60–68

Contents lists available at ScienceDirect

Earth and Planetary Science Letters

www.elsevier.com/locate/epsl

Unstable AMOC during glacial intervals and millennial variability: The role of mean sea ice extent

Florian Sévellec [a,*], Alexey V. Fedorov [b]

[a] Ocean and Earth Science, National Oceanography Centre Southampton, University of Southampton, Southampton, UK
[b] Department of Geology and Geophysics, Yale University, New Haven, CT, USA

ARTICLE INFO

Article history:
Received 15 October 2014
Received in revised form 7 July 2015
Accepted 9 July 2015
Available online 13 August 2015
Editor: J. Lynch-Stieglitz

Keywords:
Atlantic meridional overturning circulation
Holocene climate stability
Dansgaard–Oeschger events
millennial climate variability
glacial–interglacial cycle

ABSTRACT

A striking feature of paleoclimate records is the greater stability of the Holocene epoch relative to the preceding glacial interval, especially apparent in the North Atlantic region. In particular, strong irregular variability with an approximately 1500 yr period, known as the Dansgaard–Oeschger (D–O) events, punctuates the last glaciation, but is absent during the interglacial. Prevailing theories, modeling and data suggest that these events, seen as abrupt warming episodes in Greenland ice cores and sea surface temperature records in the North Atlantic, are linked to reorganizations of the Atlantic Meridional Overturning Circulation (AMOC). In this study, using a new low-order ocean model that reproduces a realistic power spectrum of millennial variability, we explore differences in the AMOC stability between glacial and interglacial intervals of the 100 kyr glacial cycle of the Late Pleistocene (1 kyr = 1000 yr). Previous modeling studies show that the edge of sea ice in the North Atlantic shifts southward during glacial intervals, moving the region of the North Atlantic Deep Water formation and the AMOC also southward. Here we demonstrate that, by shifting the AMOC with respect to the mean atmospheric precipitation field, such a displacement makes the system unstable, which explains chaotic millennial variability during the glacials and the persistence of stable ocean conditions during the interglacials.

1. Introduction

A striking feature of paleoclimate records of the last glacial interval is the strong irregular millennial variability in the North Atlantic, known as the Dansgaard–Oeschger (D–O) events (GRIP Members, 1993; Dansgaard et al., 1993; Bond et al., 1999; Alley, 2000), which contrasts the greater stability of the Holocene epoch (Fig. 1A and Grootes et al., 1993). Over the North Atlantic ocean, the D–O events occurred as a rapid warming of 5–10 °C lasting over a few decades and followed by a gradual cooling over several centuries (Bond et al., 1997; Broecker et al., 1990; Rahmstorf, 2002; Bard, 2002).

There are a number of mechanisms proposed in the past several decades to explain this variability. Prevailing theories, modeling and data suggest that the warm and cold phases of these events correspond to the strengthening and weakening of the Atlantic Meridional Overturning Circulation (AMOC) (Broecker et al., 1990; Maslin et al., 2001; Seager and Battisti, 2007), with a possible active role of the Southern Ocean winds through oceanic remote effects (Arzel et al., 2010; Banderas et al., 2012). These or similar ideas remain prevalent even though the mean AMOC strength during the last glacial interval might have been not too different from the present (Böhm et al., 2015). It is the potential bistability of the AMOC that immediately hints to the possibility that cold and warm climate states are related to the AMOC reorganization (McManus et al., 2004; Stommel, 1961; Sévellec and Fedorov, 2011). Experiments with idealized coupled ocean–atmosphere–ice models of various complexities confirm the possibility of millennial oscillations linked to an oceanic internal mode of the AMOC (Winton, 1993; Sakai and Peltier, 1999; Colin de Verdière, 2007), while other studies simulate D–O events as forced ocean response to varying freshwater fluxes (Ganopolski and Rahmstorf, 2001; Timmermann et al., 2003; Kaspi et al., 2004). Other studies also point to the contribution of sea ice and/or ice shelf dynamics to the D–O events (Gildor and Tziperman, 2000; Li et al., 2005, 2010; Dokken et al., 2013; and Petersen et al., 2013).

While demonstrating the possibility of an oceanic internal mode of the AMOC resulting in millennial variability, many studies activate this mode by increasing freshwater fluxes over the high-latitude North Atlantic ocean to unrealistically high values (e.g. Colin de Verdière et al., 2006; Sévellec et al., 2010), although ac-

* Corresponding author at: Ocean and Earth Science, University of Southampton, Waterfront campus, European Way, Southampton, SO14 3ZH, UK. Tel.: +44 2380 594850.
E-mail address: florian.sevellec@noc.soton.ac.uk (F. Sévellec).

http://dx.doi.org/10.1016/j.epsl.2015.07.022

tual changes in the Evaporation–Precipitation fields between the last glacial interval and the present are shown to be relatively weak and actually of a different sign (Kim et al., 2003, 2008; Laîné et al., 2009). This led researchers to search for other explanations of how this millennial variability can be activated. For instance, it has been proposed that a change in wind patterns, related to the expansion of Northern Hemisphere ice sheets during the glacial interval (Roe and Lindzen, 2001), can modify ocean circulation locally in the North Atlantic (Wunsch, 2006). These large continental ice sheets may have also led to the onset of the bistable regime of the AMOC (Zhang et al., 2014).

In our study we propose an alternative explanation for how the millennial AMOC variability can be activated. We will demonstrate that there is no need to change surface oceanic boundary conditions during the glacial interval (significantly increasing freshwater fluxes), in order to induce AMOC variability representative of D–O events. Relying on a series of previous studies (e.g. Arzel et al., 2010; Colin de Verdière and te Raa, 2010), we hypothesize that it is the southward shift of the North Atlantic deep-water formation, following the southward sea ice expansion, that can lead to the AMOC millennial variability (consistent with Zhang et al., 2014). Consequently, the major goal of our study is to test this hypothesis in an idealized model of the AMOC based on basic physical principles valid on long timescales.

The goal of this study is to investigate changes in the AMOC stability throughout the 100 kyr glacial–interglacial cycle that may result in climate alternating between intervals with strong millennial variability and nearly steady conditions. Our main tool is an idealized 3-degree-of-freedom loop model of the AMOC that reproduces many properties of the observed D–O events realistically (e.g. Fig. 1C, insert). To study the stability properties of the model, we will use the Pullback attractor, which provides an extension of the strange attractor approach to a non-autonomous system. Using this approach, we will show that the key time-varying parameter of the model is the southernmost extent of sea ice cover. Modifying the latitudinal structure of atmospheric precipitation that the AMOC feels, this parameter controls the stability properties of the system.

2. Model and experimental design

2.1. Model

The ocean model we employ (Sévellec and Fedorov, 2014) represents a modified version of the Howard–Malkus loop (Howard, 1971; Malkus, 1972) (Fig. 2A) where the AMOC is approximated as a rotational motion on the depth-latitude plane, neglecting spatial deformations of the zonally-averaged velocity field (i.e. neglecting changes in the isopycnal depth, see Appendix A for further details). The three model variables are anomalies in the AMOC overturning rate (ω) and ocean vertical and meridional salinity gradients (S_{BT} and S_{NS}, respectively), each depending on time (t). We assume that the steady component of the circulation (denoted Ω_0) is set by mean oceanic temperature gradients and surface winds, especially those in the Southern Ocean, and the variable part of circulation (denoted ω) is controlled by salinity gradients; the total overturning rate is $\Omega = \Omega_0 + \omega$, where Ω, Ω_0 and ω are measured in yr^{-1}.

$$d_t\omega = -\lambda\omega - \epsilon\beta S_{NS},$$

$$d_t S_{BT} = +\Omega S_{NS} - K S_{BT} + F_{BT},$$

$$d_t S_{NS} = -\Omega S_{BT} - K S_{NS} + F_{NS}.$$

Approximating oceanic circulation as a sum of (i) constant circulation controlled by surface winds and temperature gradients and (ii) variable circulation controlled by the salinity gradient is a classic assumption that goes back to the work of Stommel (1961). It relies on the fast adjustment between atmospheric and oceanic surface temperatures; therefore, temperature gradients can be considered fixed and driving, along with the wind stress, a constant oceanic flow.

This set of equations describes temporal variations of the AMOC coupled to variations in salinity. The first equation gives the momentum balance, where acceleration is controlled by buoyancy torque (with the coefficient ϵ and the haline contraction coefficient β) and linear friction (with the coefficient λ). The two other equations describe the evolution of the salinity gradients driven by advection, linear damping (with the coefficient K), and surface salt fluxes (with two components F_{BT} and F_{NS} representing the Fourier projections of surface salt flux, see Appendix A). For simplicity, we use virtual salt rather than freshwater fluxes. As discussed next, during glacial intervals this model simulates chaotic millennial variability whose spectral signature agrees well with the observations.

2.2. Experimental design

The key assumption of this study is that glacial–interglacial variations in sea ice cover push back and forth the northernmost extent of the AMOC (Eisenman et al., 2009; Arzel et al., 2010; Colin de Verdière and te Raa, 2010). In the North Atlantic the southern edge of sea ice is located at about 70°N during interglacials but can move as far as 55°N at the peak of glacial intervals (Braconnot et al., 2007; Otto-Bliesner et al., 2007) – one should expect a comparable shift in deep-water formation that controls the northern extent of the AMOC (Hewitt et al., 2003; Eisenman et al., 2009; Arzel et al., 2010; Colin de Verdière and te Raa, 2010). This is because deep water is formed primarily due to heat loss from a relatively warm surface ocean to the cold atmosphere. The heat loss is reduced significantly by the insulating effect of sea ice. There are indications of the AMOC shift in the PMIP2 simulations (Otto-Bliesner et al., 2007) – the maximum of the overturning circulation shifts southward by 5–15 degrees, depending on the model. However, those climate models were integrated for a relatively short time (several hundred years) insufficient to complete the adjustment of the AMOC (several thousand years required). Alongside these numerical experiments, observational data also suggests a possible southward shift of deep-water formation from the Nordic Sea to the region south of Iceland (Rahmstorf, 2006; Duplessy et al., 1988; Sarnthein et al., 1994).

One of the important consequences of this meridional shift of deep-water formation and the entire overturning circulation is the relative displacement of the mean atmospheric precipitation field with respect to the AMOC (changes in absolute precipitation rates being less important, Kim et al., 2003; Otto-Bliesner et al., 2007; Kim et al., 2008; Laîné et al., 2009). This is a key assumption of our study. Unlike previous authors (e.g. Sévellec et al., 2010) who increase freshwater flux into the ocean to unrealistically high values, here we assume that the precipitation field is constant and then explicitly consider the southward shift of deep-water formation. Thus, we test the hypothesis that the onset of the AMOC millennial variability can be related solely to the southward expansion of sea ice during glacial intervals.

For the same reason, to concentrate on our hypothesis, we will neglect any changes in wind stress. The wind stress can affect ocean circulation in two different ways – by modifying the imposed circulation (Ω_W) locally and by modifying the depth of the pycnocline (h) through remote effects of the Southern Ocean winds (e.g. Sévellec and Fedorov, 2011; Nikurashin and Vallis, 2012). The former effect, related to Ekman transport and hypothesized to be important for triggering D–O events (Wunsch, 2006), accounts only for ~10% of the total overturning circulation

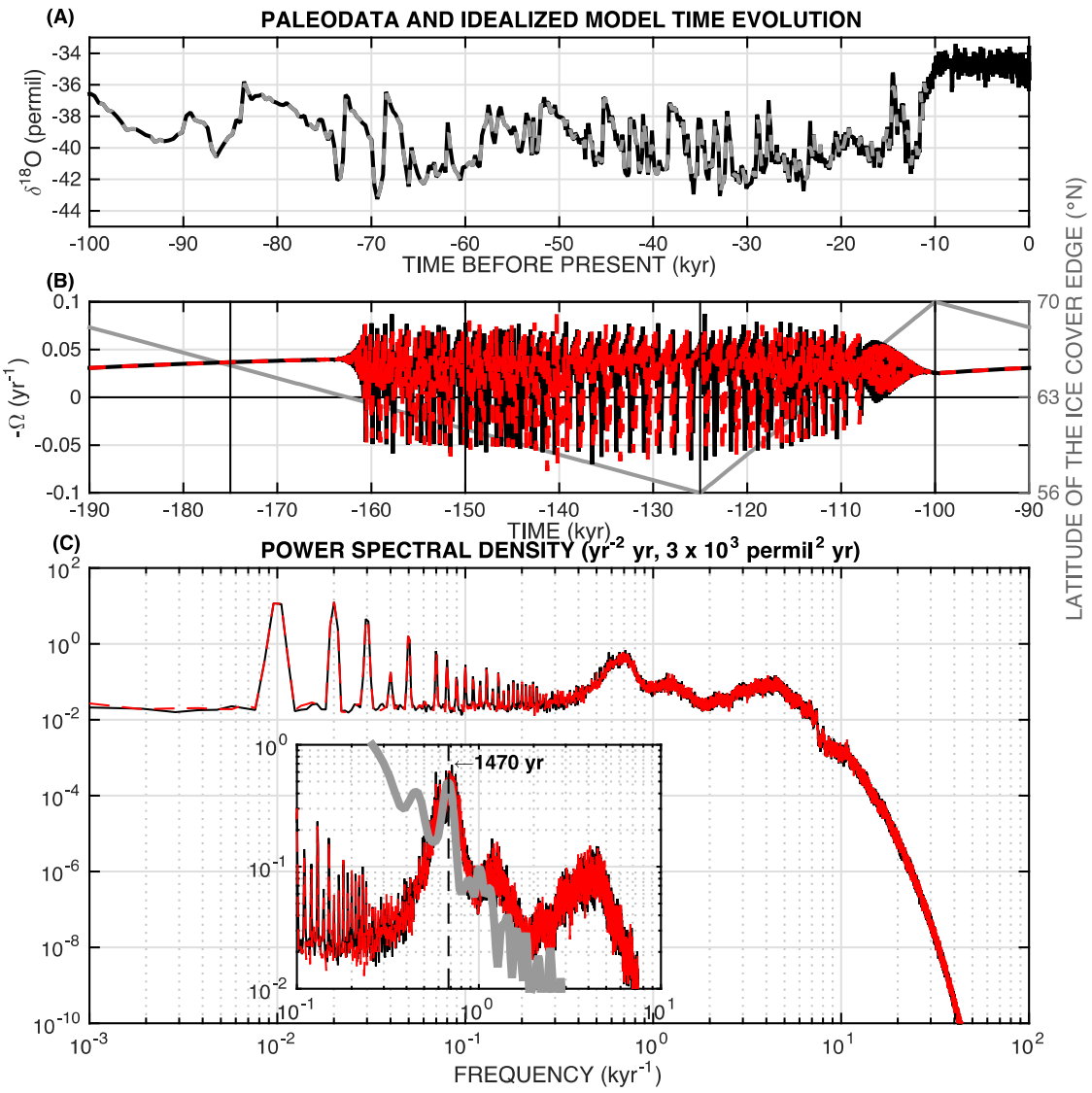

Fig. 1. Greenland δ^{18}O paleodata and AMOC variations in the loop model. (A) δ^{18}O from Greenland ice cores records (solid black and grey dashed lines) over the last 100 kyr (Grootes and Stuiver, 1997). (B) Simulated variations in the overturning rate $(-\Omega)$ for two slightly different sets of initial conditions (solid black and red dashed lines) for a single glacial–interglacial cycle. The grey sawtooth line indicates the imposed temporal changes in the position of the edge of sea ice (ESI). The four vertical lines indicate the freezing times (t_0) used later to compute the Pullback attractor. (C) The power spectra of the simulated records. The two broad spectral peaks correspond to the millennial and centennial variability; narrower peaks correspond to the 100 kyr forcing and its higher harmonics. The smaller panel highlights millennial timescales and includes the spectrum of an observed δ^{18}O signal (grey line). The vertical dashed line denotes the spectral peak corresponding to D–O events (Schulz, 2002). The model does not capture the lower-frequency variability that depends on other components of the climate system.

(McCarthy et al., 2012), so that its changes cannot impact the circulation significantly (even setting Ω_0 to zero does not alter the qualitative behavior of the model). Likewise, the pycnocline depth is only weakly sensitive to changes in Southern Ocean winds (e.g. Sévellec and Fedorov, 2011; Nikurashin and Vallis, 2012), which supports the assumption of a constant pycnocline. A further discussion is provided in Appendix A. Sensitivity experiments modifying such parameters as the mean circulation strength or the pycnocline depth do not show qualitative or any significant quantitative changes in the behavior of the idealized model.

To investigate the leading-order effect on the AMOC of such relative shifts in precipitation field, we use a fixed sinusoidal profile of virtual surface salt flux (a function of latitude) but move the boundaries of the model basin southward during the glacials (Fig. 2B, C). The time dependence of these changes is described by a sawtooth function with a zero mean and a period of 100 kyr (grey line in Fig. 1B), chosen to mimic a typical glacial–interglacial cycle of the Late Pleistocene. This time dependence leads to corresponding periodic variations in the Fourier amplitudes F_{BT} and F_{NS} (when the edge of sea ice reaches 70°N, F_{NS} is equal to the total surface salt flux and $F_{BT} = 0$, and *vice versa* when the edge of sea ice reaches 55°N; such variations conserve ocean mean salinity).

3. Results

3.1. Direct time integration

Time integrations of the equations show that the AMOC strength $(-\Omega)$ varies little during interglacial intervals, but undergoes spontaneous chaotic bursts during glacial intervals (Fig. 1B). A spectral analysis reveals a broad peak in the millennial band, around 1470 yr, consistent with the power spectrum of the observed δ^{18}O signal (Grootes and Stuiver, 1997; Schultz, 2002) (Fig. 1C). This millennial variability is associated with the quasi-periodic weakening and then strengthening of the AMOC during

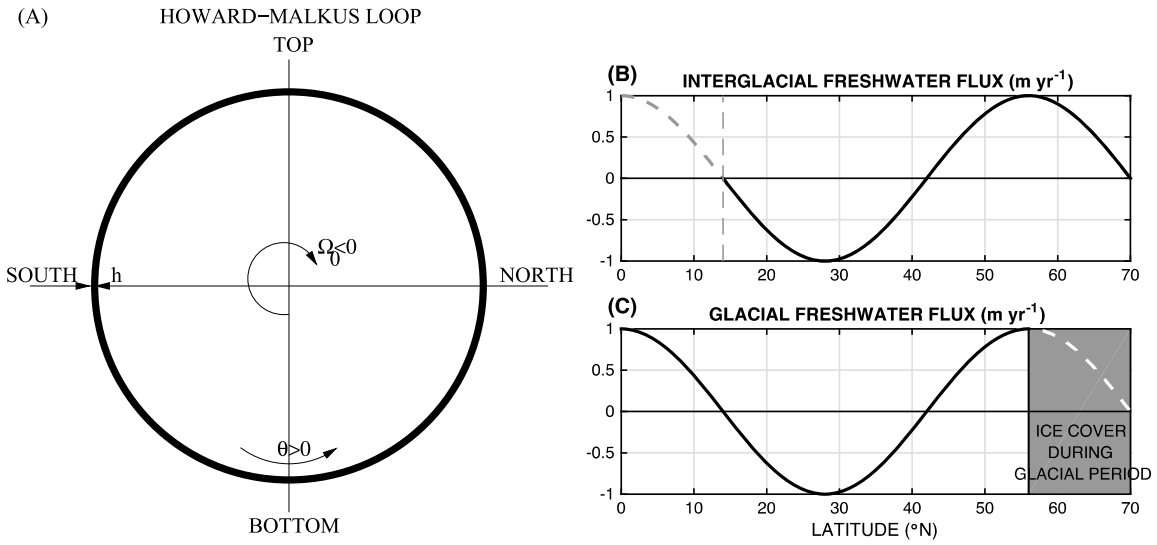

Fig. 2. A schematic of the loop model. (A) The AMOC is described as a rotational circulation following a streamline on the meridional plane. (B, C) The idealized shape of surface freshwater flux in the Atlantic as used in the loop model and the maximum extent of sea ice cover in the Northern Hemisphere during glacial intervals. The solid line represents the actual freshwater flux into the ocean used in the model for (B) interglacial and (C) glacial intervals. The dashed line indicates atmospheric freshwater forcing not impacting the ocean, either because it is south of the region of interest during the interglacials or because it is masked by sea ice during the glacials.

glacial intervals, which represents D–O events in the model. The chaotic nature of the simulated millennial variability makes the term "event" (rather than oscillation) particularly appropriate here.

Note that a spectral peak in a centennial band (200 to 250 yr) is associated with the AMOC advective timescale as given by $\sim 2\pi/\Omega_0$. Other, narrower spectral peaks correspond to the 100 kyr period of forcing and its higher harmonics (sawtooth curve in Fig. 1B).

It has been demonstrated in a previous study using the same model (Sévellec and Fedorov, 2014) that in an autonomous framework the millennial variability occurs through an infinite period bifurcation. This means that depending on model parameters the period could go from ∼1 kyr to infinity. Thus, it is particularly important to set the model parameters to realistic values (see Appendix A for further discussion and estimates of realistic set of parameters that generate a spectral peak at 1470 yr).

The AMOC in the simulated millennial variability alternates between the on- and off-states (positive and negative values in Fig. 1B). When a sufficient amount of freshwater accumulates in the North, the circulation slows down due to positive salinity feedbacks acting to weaken the overturning (Sévellec et al., 2010; Marotzke, 1996). After the circulation collapses, salt accumulates in the upper ocean, reducing ocean stratification. When the stratification becomes unstable, ocean circulation rapidly reactivates. Then the cycle repeats, leading to millennial variability (Sévellec et al., 2010). Superimposed on the millennial oscillation is centennial variability important for the transition between different AMOC states (Sévellec et al., 2006, 2010).

This general behavior is similar to the "deep-decoupling" oscillations present in a range of simple and more complex models (e.g. Winton, 1993; Winton and Sarachik, 1993; Colin de Verdière et al., 2006; Sévellec et al., 2010). While this deep-decoupling is often achieved by unrealistically increasing freshwater flux into the ocean, it provides a consistent and robust representation of AMOC millennial variability, and of D–O events, independent from the details of model configurations. Within the deep-decoupling oscillations, ocean stratification is reduced primarily by the warming of the deep ocean (Winton and Sarachik, 1993). However, in terms of ocean vertical stratification, this warming is equivalent to an increase in the upper-ocean salt content. Therefore, despite simplifications of our idealized model (the absence of explicit temperature), the AMOC resumption mechanism is generally consistent

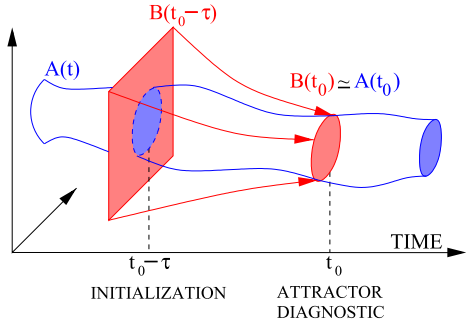

Fig. 3. A sketch for computing the Pullback attractor. $A(t)$ is the a priori unknown non-autonomous attractor of the system, $B(t_0-\tau)$ is a large number of randomly selected initial conditions in the phase space. Time $t_0-\tau$ is the integration starting time, and t_0 is the freezing time (the time when the Pullback attractor is diagnosed). The arrows show trajectories of the system $B(t)$ in the phase space. The duration of integration τ is chosen such that by time t_0 the system trajectories converge to $A(t_0)$.

with the previous analyses. Thus, as also explained in Sévellec and Fedorov (2014), our idealized model is able to reproduce the main characteristics of the deep-decoupling oscillations as described in other models.

3.2. Pullback attractor

Next, to understand why spontaneous chaotic bursts appear only during glacial intervals, we will examine the attractor of this non-autonomous system in the Pullback sense (Ghil et al., 2008; Chekroun et al., 2011). The Pullback attractor is a generalization of strange attractors for non-autonomous systems (i.e. evolving in time). To find a Pullback attractor for a particular system, one needs to integrate the equations of motion over a chosen time interval using a large number of different initial conditions (Fig. 3). By the end of integration (at the "freezing" time), computing the probability density function of the system positions in the phase space gives the Pullback attractor (assuming that the system trajectories converge, the attractors should not depend on the integration length, see Appendix B).

Note that perturbing initial conditions to determine the probability of the system future states is analogous to ensemble experiments extensively used with climate GCMs. However, in GCM

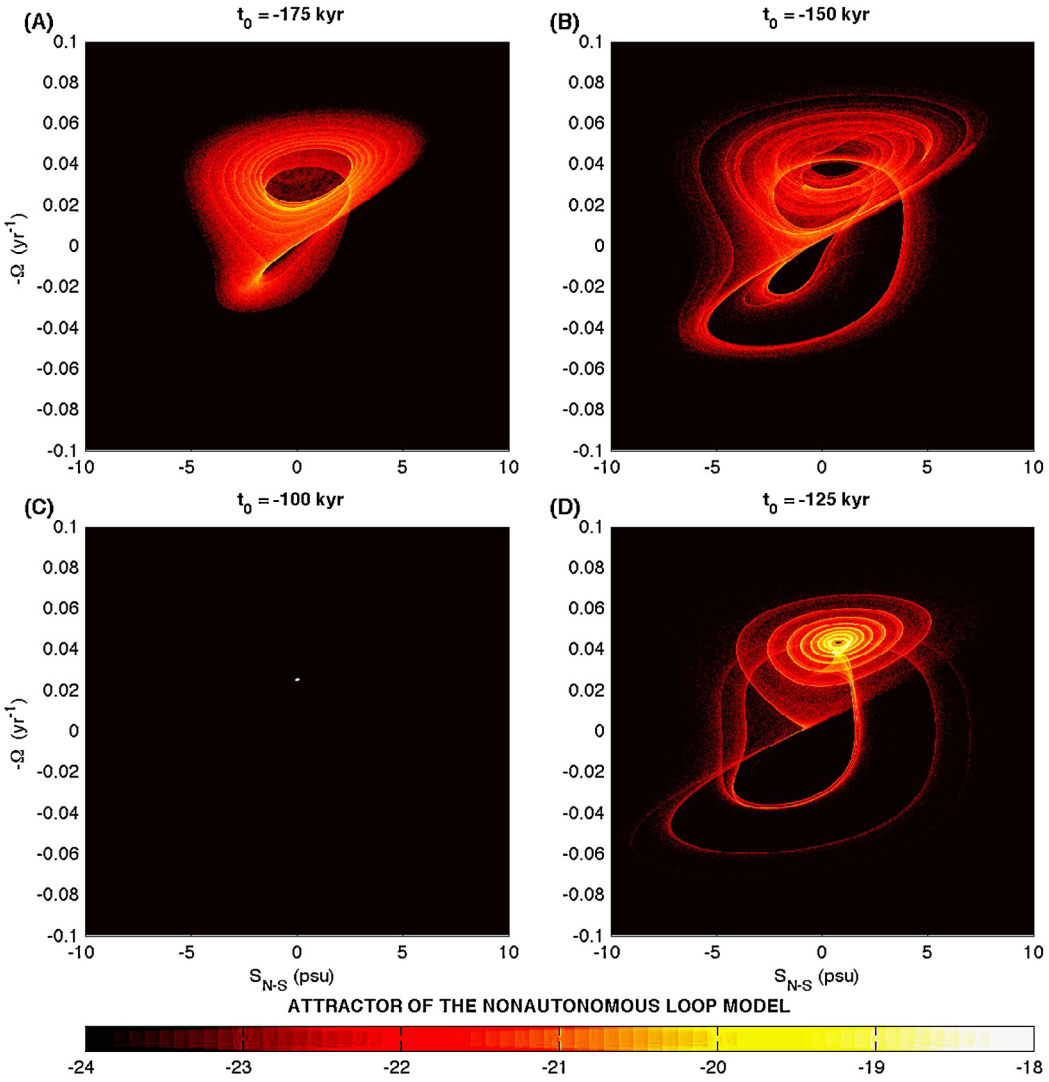

Fig. 4. Attractors of the loop model in the Pullback sense. (A)–(D) The Pullback attractors computed for different freezing times $t_0 = -175$ kyr, -150 kyr, -125 kyr, and -100 kyr (clockwise), which covers the full span of a glacial–interglacial cycle. Colors represent the probability density function for the system positions in the phase space at the end of integration; note the log scale. Computations start 5 kyr before t_0. The attractor for $t_0 = -100$ kyr in panel (C) is given by a single point, which indicates that during the interglacials the system is stable and insensitive to initial conditions.

experiments the total number of ensemble members is typically small due to computational limitations and hence inadequate to evaluate the proper statistics. In contrast, to find a Pullback attractor for our idealized model, we use a very large number of experiments (2×10^6), each with different initial conditions. Computing the Pullback attractor for our idealized model is numerically as expensive as computing several decades for a state-of-the-art ocean GCM.

To study how the stability properties of the system change within the glacial–interglacial cycle, we have computed Pullback attractors for twenty different freezing times (separated by 5 kyr, see supporting information Movie M1), but here we focus only on four freezing times separated by 25 kyr (vertical lines in Fig. 1B). Our computations reveal two different regimes. The first regime, characteristic of the interglacial (freezing time $t_0 = -100$ kyr), shows no sensitivity to initial conditions (Fig. 4C), which implies the system stability. The second regime, characteristic of the glacial interval ($t_0 = -125$, 150, 175 kyr), shows a strong sensitivity to initial conditions and a much greater uncertainty of the position of the system in the phase space (Fig. 4A, B, D), which implies the system instability. (The degree of the uncertainty and the attractor's shape depend on a particular choice of t_0.)

An essential property of the Pullback approach is its ability to provide probabilistic predictions (Ghil et al., 2008; Chekroun et al., 2011). In fact, the probability density distributions in Fig. 4 (and supporting information Movie M1) give the probability to find the system in a particular state of the phase space. For instance, for several millennia around time $t_0 = -100$ kyr (during the interglacial), we have a 100% chance to find the overturning rate equal to $-\Omega \simeq 2.5 \times 10^{-2}$ yr^{-1} (white dot, Fig. 4C). At $t_0 = -125$ kyr (around the glacial maximum), there is a significant probability to observe ocean states near $-\Omega \simeq 4.5 \times 10^{-2}$ yr^{-1}, with a stronger circulation (Fig. 4D). However, for the latter time the attractor shows a much greater uncertainty, and the system has a nontrivial chance to have overturning rates $-\Omega$ between 0 and 5×10^{-2} yr^{-1}, or even negative values (circulation collapse). This implies that D–O events have higher probability around -125 kyr. It is also the time that D–O events can potentially achieve higher amplitude (compared to -150 kyr, for instance). After -125 kyr the attractor contracts (to zero at -100 kyr) suggesting that D–O events at the end of the glacial period will be significantly weaker. This is consistent with the observed reduction in variability between -27 and -15 kyr before present in δ^{18}O (Fig. 1A).

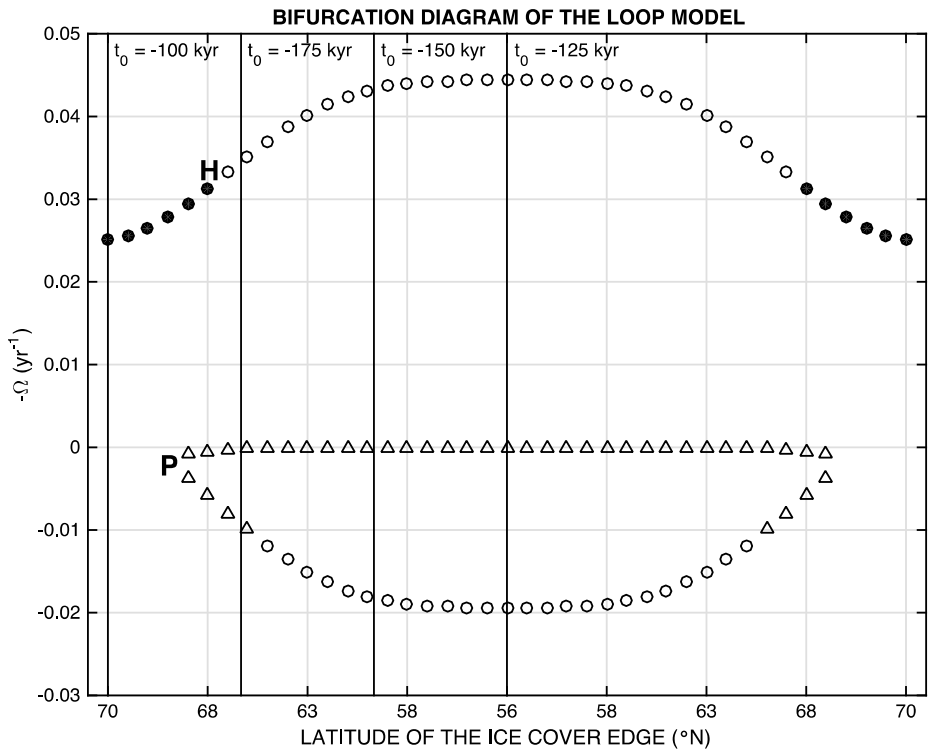

Fig. 5. A bifurcation diagram of the loop model. The diagram shows different steady states of the system (in terms of overturning strength $-\Omega$) as a function of the position of the edge of sea ice (ESI). The system is treated as autonomous, and the ESI latitude is used as the control parameter. The pitchfork and Hopf bifurcations on the diagram are denoted by letters P and H, respectively. Filled and open symbols represent stable and unstable steady states, respectively. The shape of the symbols indicates whether the most unstable eigenmode of a steady state exhibits oscillatory behavior (circles) or not (triangles). The horizontal axis runs from 70°N to 56°N and back. Solid vertical lines indicate the extent of sea ice at the freezing times (t_0) for which the Pullback attractor was computed in Fig. 4.

Consequently, the Pullback attractor shows some predictive skills. For example, at −175 kyr, the Pullback attractor in Fig. 4A is already sufficiently expanded while the two trajectories presented in Fig. 1B barely show any differences. This is because for the latter figure the two trajectories are not randomly chosen in the phase space – they both come from the same region of the phase spaces (i.e. the two trajectories are superposed from −165 kyr onwards) and their initial difference is extremely small. Hence, by accurately sampling the entire phase space, the Pullback attractor is able to assess the future chaotic behavior of the trajectories.

3.3. *Model bifurcation diagram in autonomous approximation*

Our results suggest that, to the leading order, the computed Pullback attractors depend only on the position of the edge of sea ice (ESI). For example, attractors obtained for $t_0 = -112.5$ and $t_0 = -162.5$ kyr (not shown here) turn out to be very similar – both correspond to the ESI at 63°N. Consequently, since the timescales of millennial variability are much shorter than the 100 kyr period of the glacial cycles, the system can be treated as a succession of steady, possibly unstable states, each corresponding to a particular ESI latitude, which allows studying the stability of the model within a simplified, autonomous framework. Thus, we have constructed a bifurcation diagram for the model with the ESI position as a control parameter (Fig. 5). For this diagram, we have obtained steady-state solutions of the model equations and examined their linear stability using conventional methods (Strogatz, 1994).

The stability analysis reveals an imperfect pitchfork bifurcation (Strogatz, 1994) occurring when the ESI latitude moves sufficiently far south (to ∼69°N, indicated by letter P in Fig. 5). Before this bifurcation the system has a single stable steady state, whereas after the bifurcation it has one stable steady state (coming from the same branch) and two unstable steady states. A second bifurcation occurs when the ESI reaches ∼68°N (indicated by letter H in Fig. 5), and the stable steady states branch becomes unstable (Hopf bifurcation, Strogatz, 1994). Consequently, for sea ice cover typical of interglacial intervals, there is a single stable steady state. However, for glacial intervals, there exist three unstable steady states. The system trajectory becomes chaotic in this latter regime and wanders in the phase space between the three unstable steady states, leading to millennial variability. (Note that the exact occurrence of the bifurcation does not coincide with the transition between the interglacial and glacial intervals.)

These results help to understand the shape of the non-autonomous attractors in Fig. 4. Indeed, for $t_0 = -100$ kyr (ESI = 70°N) all initial conditions converge to one positive value of Ω, which is consistent with the bifurcation diagram having a single stable steady state. In contrast, for all other Pullback attractors the trajectories undergo centennial oscillations around positive AMOC, which is consistent with the oscillatory behavior of the most unstable eigenmode of the unstable steady state. There is a strong agreement between the general predictions of the Pullback attractor (Fig. 4) and the bifurcation diagram (Fig. 5). In particular at −175 kyr (ESI = 66°N), both diagnostics suggest an incoming chaotic behavior, not yet visible in the direct time integrations (Fig. 1B). Further, the size of the attractor in the phase space is related to the system's proximity to the pitchfork bifurcation. For example, for $t_0 = -175$ kyr (ESI = 66°N) the ghost of the stable steady state attracts the trajectory more efficiently than for $t_0 = -150$ kyr and −125 kyr (ESI = 60°N and 56°N).

4. Conclusion

In summary, we have formulated an idealized loop model that describes realistic chaotic millennial variability of the AMOC as we

shift the mean precipitation field relative to the oceanic meridional overturning. Although the model is extremely simple, it shows a surprisingly rich dynamical behavior that accounts for many properties of the observed D–O events and the climate record of the last ∼100 kyr and, in particular, reproduces its spectral behavior realistically. The critical time-varying parameter of the model is the southernmost extent of sea ice cover. Modifying the latitudinal structure of atmospheric precipitation that the ocean meridional overturning circulation is exposed to, this parameter controls the stability properties of the system. Using the Pullback attractor approach, we show that only during interglacials can the system maintain a stable circulation, but during glacial intervals it shifts to an unstable chaotic regime characterized by strong millennial variability driven solely by internal oceanic dynamics.

Previously, it has been shown that sea ice can play an important role in abrupt climate changes by amplifying SST variations in response to changes in the AMOC through the ice-albedo feedback (e.g. Li et al., 2005; Dokken et al., 2013). In that context, sea ice cover was treated as part of oceanic millennial variability. Here, we emphasize another important role of sea ice – on longer glacial–interglacial timescales the mean extent of sea ice in the northern high latitudes controls the effective structure of atmospheric precipitation that reaches the ocean. This becomes a key factor leading to the AMOC instability and millennial variability during the glacials.

Acknowledgements

The data for this paper are available upon request to Florian Sévellec (florian.sevellec@noc.soton.ac.uk). This research was supported by grants from DOE Office of Science (DE-SC0007037), NSF (AGS-1405272), the David and Lucile Packard Foundation, Natural and Environmental Research Council UK (MESO-CLIP, NE/K005928/1) and the Ti Ammo project funded through the French CNRS/INSU/LEFE program.

Appendix A. Model equations

The idealized model can be derived from the large-scale equations of oceanic motion – the conservation of heat and salt, the momentum equations along the three spatial directions (i.e. geostrophic balance along the zonal and meridional directions and hydrostatic balance for the vertical direction), and the conservation of mass (i.e. the non-divergence). Simplifying these equations, we invoke a linear frictional balance that relates the meridional flow, and hence the overturning mass transport, to the meridional pressure gradient. This balance is commonly used in two-dimensional zonally-averaged ocean models describing the AMOC on the latitude-depth plane (e.g., Wright and Stocker, 1991; Marotzke, 1990) and has been shown to hold well on long timescales (Wright and Stocker, 1992) and in the northern region of the North Atlantic (Sévellec and Huck, 2015) relevant to this study. Recent theoretical studies of the AMOC that incorporate the effect of Southern Ocean winds (see discussion below) also explicitly or implicitly assume that the flow is down-pressure-gradient (e.g. Gnanadesikan, 1999; Sévellec and Fedorov, 2011; Wolfe and Cessi, 2011; Nikurashin and Vallis, 2012).

In this paper, we simplify the dynamics further and reduce the problem to just one spatial dimension. To do so, we neglect the deformation of the overturning flow and consider only its rotational part by following a single streamline of the AMOC on the meridional plane. This is equivalent to neglecting variations of pycnocline depth. This simplification still allows an accurate representation of both the positive salinity feedback (Marotzke, 1996) and the centennial variability of the thermohaline circulation (Sévellec et al., 2006) – the two processes crucial for the millennial AMOC variability as discussed in Section 3.1 and in Sévellec et al. (2010).

Prevailing theories indicate that westerly winds in the Southern Ocean is a major factor of the AMOC dynamics (e.g. Toggweiler and Samuels, 1998; Gnanadesikan, 1999; Sévellec and Fedorov, 2011; Wolfe and Cessi, 2011; Haertel and Fedorov, 2012; Nikurashin and Vallis, 2012) setting the pycnocline depth in the Atlantic Ocean via the competition between eddy buoyancy fluxes and advection by the mean Eulerian meridional circulation in the Southern Ocean. Assuming that the flow is largely rotational and its mean component (Ω_0) does not vary, we implicitly neglect changes in the Southern Ocean winds between glacial and interglacial intervals, which is justified by the relatively low sensitivity of the pycnocline depth to the zonal wind stress intensity (e.g. Sévellec and Fedorov, 2011 or Nikurashin and Vallis, 2012).

To describe the rotational flow mathematically, we can place ourselves in the center of the ocean basin, inside a simple, closed curve formed by the chosen streamline (Fig. 2). We then introduce the angle θ, positive for counterclockwise motion and measured from the ocean bottom, as the new spatial coordinate. The flow intensity (overturning rate) will not vary with θ since the flow is incompressible. In this framework, the meridional density gradient acts as a buoyancy torque for the overturning circulation. For further details, we refer the reader to Sévellec and Fedorov (2014), where this idealized model was first introduced to study the AMOC millennial variability.

The flow is described by a single variable Ω forced by buoyancy torque and surface winds stress, and affected by friction. Accordingly, the momentum equation for the loop model is written as

$$d_t\Omega = -\lambda\Omega - \frac{\epsilon}{\rho_0}\int_0^{2\pi}\rho\sin\theta d\theta,$$

where Ω is the total overturning circulation rate, θ – the direct (counterclockwise) angle around the loop measured from the ocean bottom, t – time, ρ – the density anomaly, ρ_0 – the reference density, ϵ – a proportionality factor connecting the overturning circulation to buoyancy torque (represented by the integral), and λ – a friction coefficient parameterizing turbulent viscosity in the ocean. Since the flow is incompressible, Ω does not vary with θ.

Temperature and salinity, T and S, evolve according to advective–diffusive equations:

$$\partial_t T + \Omega\partial_\theta T = K\partial_\theta^2 T + \gamma\left(T^* - T\right),$$
$$\partial_t S + \Omega\partial_\theta S = K\partial_\theta^2 S + F\frac{S_0}{h},$$

where K is eddy diffusivity, γ^{-1} – the thermal restoring timescale, T^* – the atmospheric temperature, F – the surface freshwater flux, and h – the effective depth of the flow along the loop (is set as a constant and, due to its relation to the pycnocline depth, corresponds to assuming no change of the zonal wind over the Southern Ocean). The freshwater flux is converted into a virtual salinity flux.

The system is closed by using a linear equation of state that relates density to temperature and salinity:

$$\rho = \rho_0\left[1 - \alpha(T - T_0) + \beta(S - S_0)\right],$$

where T_0 is a reference temperature, S_0 – a reference salinity, α – the thermal expansion coefficient, and β – the haline contraction coefficient.

Following Marotzke (1990), we assume that the thermal restoring timescale (∼1 month) is much faster than the advective (∼100 yr) and diffusive timescales (∼1 kyr). This suggests that temperature can be considered being close to equilibrium when

studying centennial and longer AMOC variations. In such an approximation, ocean temperature T, is set solely by the atmospheric temperature T^*, so that $T = T^*$. This allows simplifying the system by eliminating the temperature equation.

Using the linear equation of state and separating the constant and variable parts in the momentum equation, we obtain two independent equations for the overturning rate:

$$\Omega_0 = \Omega_W + \frac{\epsilon}{\lambda}\int_0^{2\pi} \alpha T^* \sin\theta d\theta,$$

$$d_t\omega = -\lambda\omega - \epsilon\int_0^{2\pi} \beta S \sin\theta d\theta,$$

where $\Omega = \Omega_0 + \omega$, Ω_0 is a constant representing the temperature-plus wind-induced circulation Ω_W, and ω a variable value representing the salinity-induced circulation.

Ω, Ω_0 and ω are measured in the units of yr^{-1} and reflect the rate of ocean overturning. These equations imply that the steady circulation is set by atmospheric temperature and winds, whereas variations are set by salinity. Subsequently, the steady circulation can be treated as an external parameter.

Thus, we have obtained a closed set of equations:

$$d_t\omega = -\lambda\omega - \epsilon\int_0^{2\pi} \beta S \sin\theta d\theta,$$

$$\partial_t S + \Omega\partial_\theta S = K\partial_\theta^2 S + F\frac{S_0}{h}.$$

The periodicity of the loop allows us to use a Fourier decomposition for S such that

$$S(t,\theta) = \Re\left[\sum_{n\in\mathbb{N}} S_n(t)e^{in\theta}\right],$$

where $\Re$ indicates the real part,

$$S_n = S_{rn} + iS_{in} = \frac{1}{2\pi}\int_0^{2\pi} Se^{-in\theta}d\theta,$$

and the subscripts r and i stand for the real and imaginary parts, respectively.

Since the sine-like structure of the freshwater forcing projects only on the first mode (S_1), we restrict our study to this first Fourier mode. S_1 is associated with the gravest Fourier mode, thus the real and imaginary parts of S_1 are associated with the projections of salinity field onto $\cos(\theta)$ and $\sin(\theta)$. $\theta = 0$ is located at the maximum depth and the angle increases counterclockwise (Fig. 1A); we have at the Bottom $\cos(\theta = 0) = 1$ and $\sin(\theta = 0) = 0$, at the North $\cos(\theta = \pi/2) = 0$ and $\sin(\theta = \pi/2) = 1$, at the Top $\cos(\theta = \pi) = -1$ and $\sin(\theta = \pi) = 0$, and at the South $\cos(\theta = 3\pi/2) = 0$ and $\sin((\theta = 3\pi/2) = -1$. Thus, the real and imaginary parts of S_1 represent the ocean bottom-top and north–south salinity gradients. We use the notation $S_{BT} = S_{r1}$ and $S_{NS} = S_{i1}$, we rewrite the equations of the incompressible loop model as:

$$d_t\omega = -\lambda\omega - \epsilon\beta S_{NS},$$
$$d_t S_{BT} = +\Omega S_{NS} - K S_{BT} + F_{BT},$$
$$d_t S_{NS} = -\Omega S_{BT} - K S_{NS} + F_{NS},$$

where $F_{BT} + iF_{NS} = \frac{S_0}{2\pi h}\int_0^{2\pi} Fe^{-i\theta}d\theta$.

That is, F_{BT} and F_{NS} are Fourier projections of the surface salt flux.

Time integration of the model equations follows a fourth-order Runge–Kutta method. Two sets of initial conditions randomly chosen in the model phase space are used for plotting Fig. 1B, C (black and red lines). This tests the system sensitivity to the initial conditions (indicating deterministic chaotic behavior). The model is integrated over 20,000 kyr (a 100 kyr glacial cycle times two hundred). For the model parameters, we use $\lambda = 10^{-2}\ \mathrm{yr}^{-1}$, $\epsilon = 3.5\times10^{-1}\ \mathrm{yr}^{-1}$, $\beta = 7\times10^{-4}\ \mathrm{psu}^{-1}$, $\Omega_0 = -2.5\times10^{-2}\ \mathrm{yr}^{-1}$, $K = 10^{-4}\ \mathrm{yr}^{-1}$, $|F| = 1\ \mathrm{m\,yr}^{-1}$ (the magnitude of the surface salt flux), $S_0 = 35$ psu, and $h = 1000$ m. These values are set using the relevant observations, e.g. 1000 m is chosen as the typical depth of the pycnocline. On the other hand, λ is set by the timescale over which the *ad hoc* frictional balance is achieved, which implies a meridional adjustment of the ocean; we estimate this timescale at 100 yr (see Sévellec and Fedorov, 2014, for a detailed description). Finally ϵ is an *ad hoc* parameter relating the meridional pressure gradient to the meridional flow; it is set to give a realistic density contrast for a realistic overturning flow in a steady state.

Appendix B. Computing the Pullback attractor

In order to compute the Pullback attractor at time t_0 we conduct integrations of the nonlinear equations of the loop model for a very large number (N) of randomly chosen initial conditions starting at time $t = t_0 - \tau$. After initialization the system follows a unique trajectory for each set of initial conditions. At time t_0 we freeze the trajectories and evaluate the positions of the system in the phase space for all different initial conditions. Mathematically, the Pullback attractor is obtained by computing the probability density function of system positions (σ) in the phase space. The measure we use is

$$\sigma(\Omega, S_{NS}, t_0) = \log\left(\frac{1}{N}\sum_{d\phi} n(\Omega, S_{NS}, t_0)d\phi\right),$$

where t_0 is the "freezing time" (the time when the attractor is diagnosed), $d\phi$ a unit area of the phase space (projected on $S_{BT} = 0$), and n the number of trajectories that entered this particular unit area. We use $N = 2\times10^6$ and the convergence delay of $\tau = 5$ kyr. These values of N and τ proved to be sufficient to obtain a good representation and adequate convergence of the attractor. Computing the Pullback attractor for our idealized model is numerically as expensive as computing several decades of state of the art Ocean GCM. Illustration of the Pullback attractor are given in Fig. 4 and supporting information Movie M1.

Appendix C. Supplementary material

Supplementary material related to this article can be found online at http://dx.doi.org/10.1016/j.epsl.2015.07.022.

References

Alley, R.B., 2000. Ice-core evidence of abrupt climate changes. Proc. Natl. Acad. Sci. USA 97, 1331–1334.
Arzel, O., Colin de Verdière, A., England, M.H., 2010. The role of oceanic heat transport and wind stress forcing abrupt millennial-scale climate transitions. J. Climate 23, 2233–2256.
Banderas, R., Álvarez-Solas, J., Montoya, M., et al., 2012. Role of CO_2 and Southern Ocean winds in glacial abrupt climate change. Clim. Past 8, 1011–1021.
Bard, E., 2002. Climate shock: abrupt change over millennial time scales. Phys. Today, 32–38.
Böhm, E., et al., 2015. Strong and deep Atlantic meridional overturning circulation during the last glacial cycle. Nature 517, 73–76.
Bond, G., et al., 1997. A pervasive millennial-scale cycle in North Atlantic Holocene and glacial climates. Science 278, 1257–1266.

Bond, G., et al., 1999. The North Atlantic's 1–2∼kyr climate rhythm: relation to Heinrich events, Dansgaard–Oeschger events, and the Little Ice Age. Geophys. Monogr. Ser. 112, 35–58.
Braconnot, P., et al., 2007. Results of PMIP2 coupled simulations of the Mid-Holocene and Last Glacial Maximum – Part 1: experiments and large-scale features. Clim. Past 3, 261–277.
Broecker, W.S., et al., 1990. A salt oscillator in the glacial Atlantic? 1. The concept. Paleoceanography 5, 469–477.
Chekroun, M., Simonnet, E., Ghil, M., 2011. Stochastic climate dynamics: random attractor and time-dependent invariant measures. Physica D 240, 1685–1700.
Colin de Verdière, A., Ben Jelloul, M., Sévellec, F., 2006. On the bifurcation structure of thermohaline millennial oscillation. J. Climate 19, 5777–5795.
Colin de Verdière, A., 2007. A simple model of millennial oscillations of the thermohaline circulation. J. Phys. Oceanogr. 37, 12–1155.
Colin de Verdière, A., te Raa, L., 2010. Weak oceanic heat transport as a cause of the instability of glacial climates. Clim. Dyn. 35, 1237–1256.
Dansgaard, W., et al., 1993. Evidence for general instability of past climate from 250-kyr ice-core record. Nature 364, 218–220.
Dokken, T.M., et al., 2013. Dansgaard–Oeschger cycles: interactions between ocean and sea ice intrinsic to the Nordic Seas. Paleoceanography 28, 491–502.
Duplessy, J.C., et al., 1988. Deepwater source variations during the last climatic cycle and their impact on the global deep water circulation. Paleoceanography 3, 343–360.
Eisenman, I., Bitz, C., Tziperman, E., 2009. Rain driven by receding ice sheets as a cause of past climate change. Paleoceanography 24, PA4209.
Ganopolski, A., Rahmstorf, S., 2001. Simulation of rapid glacial climate changes in a coupled climate model. Nature 409, 153–158.
Ghil, M., Chekroun, M., Simonnet, E., 2008. Climate dynamics and fluid mechanics: natural variability and related uncertainties. Physica D 237, 2111–2126.
Gildor, H., Tziperman, E., 2000. Sea ice as a glacial cycles' climate switch: role of the seasonal and orbital forcing. Paleoceanography 15, 605–615.
Gnanadesikan, A., 1999. A simple predictive model for the structure of the oceanic pycnocline. Science 283, 2077–2079.
GRIP Members, 1993. Climate instability during the last interglacial period recorded in the GRIP ice core. Nature 364, 203–207.
Grootes, P.M., Stuiver, M., Whire, J.W.C., Johnsen, S., Jouzel, J., 1993. Comparison of oxygen isotope records from GISP2 and GRIP Greenland ice cores. Nature 366, 552–554.
Grootes, P.M., Stuiver, M., 1997. Oxygen 18/16 variability in Greenland snow and ice with 10^3 to 10^5-year time resolution. J. Geophys. Res. 102, 26455–26470.
Haertel, P., Fedorov, A.V., 2012. The ventilated ocean. J. Phys. Oceanogr. 42, 141–164.
Hewitt, C.D., Stouffer, R.J., Broccoli, A.J., Mitchell, J.F.B., Valdes, P.J., 2003. The effect of ocean dynamics in a coupled GCM simulation of the Last Glacial Maximum. Clim. Dyn. 20, 203–218.
Howard, L.N., 1971. ABC's of convection, geophysical fluid dynamics summer school. Tech. Rep., 71-63, 102-105, WHOI internal report.
Kaspi, Y., Sayag, R., Tziperman, E., 2004. A 'triple sea-ice state' mechanism for the abrupt warming and synchronous ice sheet collapses during Heinrich events. Paleoceanography 19, PA3004.
Kim, S.-J., Flato, G.M., Boer, G.J., 2003. A coupled climate model simulation of the Last Glacial Maximum. Part 2: approach to equilibrium. Clim. Dyn. 20, 635–661.
Kim, S.-J., et al., 2008. High-resolution climate simulation of the last glacial maximum. Clim. Dyn. 31, 1–16.
Laîné, A., et al., 2009. Northern hemisphere storm tracks during the last glacial maximum in the PMIP2 ocean–atmosphere coupled models: energetic study, seasonal cycle, precipitation. Clim. Dyn. 32, 593–614.
Li, C., Battisti, D.S., Schrag, D.P., Tziperman, E., 2005. Abrupt climate shifts in Greenland due to displacements of the sea ice edge. Geophys. Res. Lett. 32, L19702.
Li, C., Battisti, D.S., Bitz, C.M., 2010. Can North Atlantic Sea ice anomalies account for Dansgaard–Oeschger climate signals? J. Climate 23, 5457–5475.
Malkus, W.V.R., 1972. Non-periodic convection at high and low Prandtl number. Mem. Soc. R. Sci. Liege, Collect. in-4 6e, 125–128.
Marotzke, J., 1990. Instabilities and multiple equilibria of the thermohaline circulation. Ph.D. thesis, Berichte aus dem Institut für Meereskunde Kiel, vol. 94. 126 pp.
Marotzke, J., 1996. Analysis of thermohaline feedbacks. In: Decadal Climate Variability, Dynamics and Predictability. In: Anderson, D.L.T., Willebrand, J. (Eds.), NATO ASI Series, Series I, vol. 44, pp. 333–378.
Maslin, M., Seidov, D., Lowe, J., 2001. Synthesis of the nature and causes of rapid climate transitions during the quaternary. In: The Oceans and Rapid Climate Change: Past, Present, and Future. In: AGU Geophysical Monograph, vol. 126, pp. 9–52.
McCarthy, G., et al., 2012. Observed interannual variability of the Atlantic Meridional overturning circulation at 26.5°N. Geophys. Res. Lett. 39, L19609.
McManus, J.F., et al., 2004. Collapse and rapid resumption of Atlantic meridional circulation linked to deglacial climate changes. Nature 428, 834–836.
Nikurashin, M., Vallis, G., 2012. A theory of the interhemispheric meridional overturning circulation and associated stratification. J. Phys. Oceanogr. 42, 1652–1667.
Otto-Bliesner, B.L., et al., 2007. Last Glacial Maximum ocean thermohaline circulation: PMIP2 model intercomparisons and data constraints. Geophys. Res. Lett. 34, L12706.
Petersen, S.V., Schrag, D.P., Clark, P.U., 2013. A new mechanism for Dansgaard–Oeschger cycles. Paleoceanography 28, 24–30.
Rahmstorf, S., 2002. Ocean circulation and climate during the past 120,000 years. Nature 419, 207–214.
Rahmstorf, S., 2006. Thermohaline ocean circulation. In: Elias, S.A. (Ed.), Encyclopedia of Quaternary Sciences. Elsevier, Amsterdam.
Roe, G.H., Lindzen, R.S., 2001. The mutual interaction between continental-scale ice sheets and atmospheric stationary waves. J. Climate 14, 1450–1465.
Sakai, K., Peltier, W.R., 1999. A dynamical systems model of the Dansgaard–Oeschger oscillation and the origin of the Bond cycle. J. Climate 12, 2238–2255.
Sarnthein, M., et al., 1994. Changes in east Atlantic deepwater circulation over the last 30,000 years: eight time slice reconstructions. Paleoceanography 9, 209–267.
Schulz, M., 2002. On the 1470-year pacing of Dansgaard–Oeschger warm events. Paleoceanography 17, 571. http://dx.doi.org/10.1029/2000PA000.
Seager, R., Battisti, D.S., 2007. Challenges to our understanding of the general circulation: abrupt climate change. In: Schneider, T., Sobel, A.H. (Eds.), Global Circulation of the Atmosphere. Princeton University Press, pp. 331–371.
Sévellec, F., Fedorov, A.V., 2011. Stability of the Atlantic meridional overturning circulation in a zonally-averaged ocean model: the effects of freshwater flux, wind stress, and diapycnal diffusivity. Deep-Sea Res. 58, 1927–1943.
Sévellec, F., Fedorov, A.V., 2014. Millennial variability in an idealized ocean model: predicting the AMOC regime shifts. J. Climate 27, 3551–3564.
Sévellec, F., Huck, T., Ben Jelloul, M., 2006. On the mechanism of centennial thermohaline oscillations. J. Mar. Res. 64, 355–392.
Sévellec, F., Huck, T., Colin de Verdière, A., 2010. From centennial to millennial oscillation of the thermohaline circulation. J. Mar. Res. 68, 597–624.
Sévellec, F., Huck, T., 2015. Geostrophic closure of the zonally-averaged Atlantic Meridional Overturning. J. Phys. Oceanogr. http://dx.doi.org/10.1175/JPO-D-14-0148.1 (accepted).
Stommel, H., 1961. Thermohaline convection with stable regimes flow. Tellus 13, 224–230.
Strogatz, S.H., 1994. Nonlinear Dynamics and Chaos with Applications to Physics, Biology, Chemistry and Engineering. Advanced Book Program. Perseus book.
Timmermann, A., Gildor, H., Schulz, M., Tziperman, E., 2003. Coherent resonant millennial-scale climate oscillations triggered by massive meltwater pulses. J. Climate 16, 2569–2585.
Toggweiler, J.R., Samuels, B.L., 1998. On the ocean's large-scale circulation near the limit of no vertical mixing. J. Phys. Oceanogr. 28, 1832–1852.
Winton, M., 1993. Deep decoupling oscillations of the oceanic thermohaline circulation. In: Peltier, W.R. (Ed.), Ice in the Climate System. In: NATO ASI Series, Series I, vol. 12. Springer Verlag, pp. 417–432.
Winton, M., Sarachik, E.S., 1993. Thermohaline oscillations induced by strong steady salinity forcing of ocean general circulation. J. Phys. Oceanogr. 23, 1389–1410.
Wolfe, C.L., Cessi, P., 2011. The adiabatic pole-to-pole overturning circulation. J. Phys. Oceanogr. 41, 1795–1810.
Wright, D.G., Stocker, T.F., 1991. A zonally averaged ocean model for thermohaline circulation. Part I: model development and flow dynamics. J. Phys. Oceanogr. 21, 1713–1724.
Wright, D.G., Stocker, T.F., 1992. Sensitivities of a zonally averaged global ocean circulation model. J. Geophys. Res. 97, 12707–12730.
Wunsch, C., 2006. Abrupt climate change: an alternative view. Quat. Res. 65, 191–203.
Zhang, X., Lohmann, G., Knorr, G., Purcell, C., 2014. Abrupt glacial climate shifts controlled by ice sheet changes. Nature 512, 290–294.